

Detection of [Ne II] Emission from Young Circumstellar Disks

I. Pascucci¹, D. Hollenbach², J. Najita³, J. Muzerolle¹, U. Gorti⁴, G. J. Herczeg⁵, L. A. Hillenbrand⁵, J. S. Kim¹, J. M. Carpenter⁵, M. R. Meyer¹, E. E. Mamajek⁶, J. Bouwman⁷

ABSTRACT

We report the detection of [Ne II] emission at $12.81\ \mu\text{m}$ in four out of the six optically thick dust disks observed as part of the FEPS *Spitzer* Legacy program. In addition, we detect a H I(7-6) emission line at $12.37\ \mu\text{m}$ from the source RX J1852.3-3700. Detections of [Ne II] lines are favored by low mid-infrared excess emission. Both stellar X-rays and extreme UV (EUV) photons can sufficiently ionize the disk surface to reproduce the observed line fluxes, suggesting that emission from Ne^+ originates in the hot disk atmosphere. On the other hand, the H I(7-6) line is not associated with the gas in the disk surface and magnetospheric accretion flows can account for at most $\sim 30\%$ of the observed flux. We conclude that accretion shock regions and/or the stellar corona could contribute to most of the H I(7-6) emission. Finally, we discuss the observations necessary to identify whether stellar X-rays or EUV photons are the dominant ionization mechanism for Ne atoms. Because the observed [Ne II] emission probes very small amounts of gas in the disk surface ($\sim 10^{-6} M_{\text{J}}$) we suggest using this gas line to determine the presence or absence of gas in more evolved circumstellar disks.

Subject headings: line: identification – circumstellar matter – planetary systems: protoplanetary disks – infrared: stars – stars: RX J1111.7-7620, PDS 66, HD 143006, [PZ99] J161411.0-230536, RX J1842.9-3532, RX J1852.3-3700

1. Introduction

Young stars are often surrounded by gas and dust disks that may succeed in forming planets. The properties and evolution of their dust and gas components are key to understanding planet formation and the diversity of extrasolar planetary systems.

Circumstellar dust has been extensively studied in young and old disks since the IRAS mission. Grain growth has been identified in disks

around stars with masses ranging from a few solar masses (Bouwman et al. 2001) down to the brown dwarf regime (Apai et al. 2005) suggesting that the first steps of planet formation are ubiquitous. Detailed mineralogy reveal chemical processing similar to those that occurred in the early solar system (see Natta et al. 2007 for a review on dust in protoplanetary disks; Alexander et al. 2007 and Wooden et al. 2007 for dust processing in the solar nebula and in disks). On the other hand, the properties and evolution of circumstellar gas are less well characterized.

Filling this gap is one of the goals of the Formation and Evolution of Planetary Systems (FEPS) *Spitzer* legacy program (Meyer et al. 2006). In two previous contributions we derived gas mass upper limits for a sample of 16 sun-like stars surrounded by optically thin dust disks and discussed implications for the formation of terrestrial, giant, and icy planets (Hollenbach et al. 2005; Pascucci et al. 2006).

¹Steward Observatory, The University of Arizona, Tucson, AZ 85721.

²University of California, Berkeley, CA 94720

³National Optical Astronomy Observatory, Tucson, AZ 85719

⁴NASA Ames Research Center, Moffett Field, CA 94035

⁵California Institute of Technology, Pasadena, CA 91125

⁶Harvard-Smithsonian Center for Astrophysics, Cambridge, MA 02138

⁷Max Planck Institute for Astronomy, Heidelberg, Germany

Here, we present high-resolution *Spitzer* spectra for the six FEPS targets with excess emission beginning at or shortward of the $8\ \mu\text{m}$ IRAC band. Their IRAC colors are consistent with those of accreting classical T Tauri stars (Silverstone et al. 2006) suggesting that these stars are surrounded by optically thick dust disks. We report the detection of the H I (7–6) line at $12.37\ \mu\text{m}$ in one system and of the [Ne II] line at $12.81\ \mu\text{m}$ in four systems (Sect. 3.1). Because Ne atoms have a large ionization potential (21.6 eV), the detection of [Ne II] lines is of particular interest to assess the role of stellar X-ray and EUV ($h\nu > 13.6\ \text{eV}$) photons on the disk chemistry and to explore the conditions for disk photoevaporation (Glassgold, Najita & Igea 2007; Gorti & Hollenbach 2007). We discuss in detail predictions from the proposed X-ray and EUV models and future observations that will be able to identify the dominant ionization mechanism (Sect. 4 and Sect. 5). Since both models find that the [Ne II] line probes small amounts of gas on the surface of circumstellar disks, we also suggest using this tracer to place stringent constraints on the presence or absence of gas in more evolved disks.

2. Observations and Data Reduction

The general properties of the 328 stars in the FEPS sample are described in Meyer et al. (2006). We summarize in Table 1 the main properties of the six FEPS sources surrounded by optically thick dust disks. In Cols. 4, 5, and 6 we give the star spectral types (SpTy), distances (d), and ages (Age). References for these quantities are provided in Col. 7. The stellar effective temperatures (T_{eff}), visual extinctions (A_V), and bolometric luminosities (L_\star) are listed in Cols. 8, 9, and 10. The last column summarizes the source X-ray luminosities (L_X).

To compute the X-ray luminosities we used the ROSAT PSPC All-Sky Survey count-rates and HR1 hardness ratios (Alcalá et al. 1997; Voges et al. 1999, 2000) following Fleming et al. (1995), and adopting the distances in Table 1. These X-ray luminosities are representative for the energy band 0.1–2.4 keV (or 120–5 Å). The errors in L_X include the uncertainties in the count-rates, HR1, and distances. Note however that the

intrinsic variability of $\log(L_X)$ due to stellar activity is larger than the quoted uncertainty and amounts to at least a few tenths of a dex (e.g. Marino et al. 2003). Our X-ray luminosities agree with values from the literature (Alcalá et al. 1997 for source 1; Mamajek et al. 2002 for source 2; Sciortino et al. 1998 for source 3; Neuhäuser et al. 2000 for sources 5 and 6). Because source 4 appears extended in the ROSAT PSPC image, we also searched for an independent measurement of its X-ray flux. Its count-rates from the XMM-Newton¹ MOS1 and MOS2 cameras in the 0.2–2 keV bandpass convert to $\log(L_X)=30.8\ \text{erg/s}$. Since an increase of 0.26 dex in luminosity could be simply due to stellar activity, we prefer to adopt the luminosity from ROSAT for consistency with the other sources.

Among the sources listed in Table 1, HD 143006 is the only one that was included in the FEPS program as part of the gas detection experiment being a known dust disk from IRAS (Sylvester et al. 1996). The other five dust disks have been recently identified by our group from IRAC/*Spitzer* photometry (Silverstone et al. 2006). The spectral energy distributions of these five systems, including photometry from IRAC and MIPS as well as IRS low-resolution spectra, are presented in Silverstone et al. (2006). Hillenbrand et al. in prep. show that single temperature blackbody fits to the 33 and $70\ \mu\text{m}$ data cannot account for the excess emission at shorter wavelengths in any of the six sources in Table 1, indicating the presence of warm inner disk material. These optically thick dust disks are also the only six FEPS sources exhibiting dust features in the *Spitzer*/IRS low-resolution spectra. Bouwman et al. (2007) present a detailed analysis of their mineralogy and find that RX J1842.9-3532 is surrounded by an almost primordial disk (flared geometry and $1\ \mu\text{m}$ -sized grains) while [PZ99] J161411.0-230536 has the most processed disk (close to flat geometry and large $5\ \mu\text{m}$ grains).

In Sect. 2.1 we describe the observations and data reduction of the high-resolution infrared spectra. We complemented the *Spitzer* data with optical spectra (Sect. 2.2) that are used to estimate mass accretion rates (Sect. 3.2).

¹XMM-Newton Serendipitous Source Catalogue, 1XMM, <http://xmmssc-www.star.le.ac.uk/>

TABLE 1
MAIN PROPERTIES OF THE TARGETED OPTICALLY THICK DUST DISKS.

ID#	Source	2MASS J ^a	SpTy	d [pc]	Age [Myr]	Ref.	T_{eff} [K]	A_V [mag]	$\log(L_*)$ [L_{\odot}]	$\log(L_x)^b$ [erg/s]
1	RX J1111.7-7620	11114632-7620092	K1	163±10	5	1,2,3	4621	1.30	0.27	30.56±0.16
2	PDS 66	13220753-6938121	K1	86±7	17	4	5228	1.22	0.10	30.20±0.09
3	HD 143006	15583692-2257153	G6/8	145±10	5	5,6,7	5884	1.63	0.39	30.14±0.17
4	[PZ99] J161411.0-230536	16141107-2305362	K0	145±10	5	8,6,7	4963	1.48	0.50	30.54±0.10
5	RX J1842.9-3532	18425797-3532427	K2	140±10	4	9,10,3	4995	1.03	0.05	30.37±0.18
6	RX J1852.3-3700	18521730-3700119	K3	140±10	4	9,10,3	4759	0.92	-0.17	30.57±0.13

^aThe 2MASS source name includes the J2000 sexagesimal, equatorial position in the form: hhmmssss+ddmmss (Cutri et al. 2003).

^bX-ray luminosities in the ROSAT 0.1–2.4 keV energy band, see Sect. 2 for details.

NOTE.—Spectral types are from optical spectroscopy with accuracy of 1 subtype. The stellar colors B–V and V–K are used in conjunction with the spectral type to estimate effective temperatures (T_{eff}). Visual extinctions (A_V) are computed from the spectral type and stellar colors. We refer to Carpenter et al. 2007 in preparation for details. Stellar luminosities are computed from the best fit Kurucz stellar models to optical and near-infrared observations of the stellar photosphere (Carpenter et al. 2007 in prep.) and the distances in this table.

References. — (1) Alcalá et al. 1995; (2) Luhman 2007; (3) Hillenbrand et al. 2007 in prep.; (4) Mamajek et al. 2002; (5) Houk & Smith-Moore 1988; (6) de Zeeuw et al. 1999; (7) Preibisch et al. 2002; (8) Preibisch et al. 1998; (9) Neuhäuser et al. 2000; (10) Neuhäuser & Forbrich 2007

2.1. High-resolution IRS Spectra

Spitzer/IRS high-resolution spectra for the 6 FEPS optically thick dust disks were obtained between August 2004 and September 2005. Observations were done in the Fixed Cluster-Offsets mode with two nod positions on-source (located at 1/3 and 2/3 of the slit length) and two additional sky measurements (1' east of the nod1 and nod2 positions) acquired just after the on-source exposures. We used these sky exposures to remove the infrared background and reduce the number of rogue pixels as described in Pascucci et al. (2006). The PCRS or the IRS Peak-up options were used to place and hold the targets in the spectrograph slit with positional uncertainties always better than 1" (1 sigma radial). Exposure times were chosen to detect a 5% line-to-continuum ratio with a signal-to-noise of 5 (see Table 2). In the following we focus on the reduction and analysis of the SH module (9.9–19.6 μm) where we detected gas lines in four out of six targets. No gas lines are detected in the wavelength range 18.7–37.2 μm that is covered by the LH module. The SH module is a cross-dispersed echelle spectrograph with a resolving power of ~ 650 in the spectral range from 9.9–19.6 μm , corresponding to a spectral resolution of 0.015 μm around 10 μm . The detector has a plate scale of 2.3"/pixel and the slit aperture has a size of 2×5 pixels, thus covering a region of $\sim 1600 \times 700$ AU around a star at 140 pc.

Data reduction was carried out as in Pascucci et al. (2006) starting from the Spitzer Science Center (SSC) S13.2.0 *droop* products. We fixed pixels marked bad in the bmask files with flag value equal to 2^9 or larger, thus including anomalous pixels due to cosmic-ray saturation early in the integration, or preflagged as unresponsive. We also inspected visually all the SH exposures to catch additional rogue pixels and found less than 5 per frame. These bad and rogue pixels were corrected using the SSC *irsclean* package as explained in Pascucci et al. (2006).

We flux calibrated the extracted spectra using nine independent observations (over four different *Spitzer* campaigns, from C21 to C24) of the bright standard star ξ Dra and the MARCS stellar atmosphere model degraded to the spectrograph's resolution and sampling². The dispersion

in the mean fluxes of these calibrators is always less than 1.5% between 10 and 20 μm . We verified the absolute flux calibration by comparing the high-resolution spectra to the low-resolution spectra from Bouwman et al. (2007) at a wavelength in between the [Ne II] and the H I(7-6) lines. We found deviations less than $\sim 10\%$ at $12.6 \pm 0.1 \mu\text{m}$, that are within the absolute photometric accuracy estimated by the SSC, for all objects except for RX J1111.7-7620. For this source the SH spectrum has 30% higher flux but maintains the same shape as the low-resolution spectrum. We verified that this higher flux is simply due to the non-zero background emission in the vicinity of the source (the sky position we acquired for the SH spectrum is too far away from the source to be representative of the nearby emission). We have also tested that the low-resolution spectra agree with the IRAC photometry at 8 μm and the MIPS photometry at 24 μm ³. Thus, to improve our flux estimates and upper limits we scaled the high-resolution spectra to the flux of the low-resolution spectra at 12.6 μm .

2.2. Optical Spectra

Optical spectra were obtained in several observing runs and with different telescopes. The spectra of HD 143006, RX J1842.9-3532, and RX J1852.3-3700 were acquired in July 2001 and June 2003 with the Palomar 60-inch telescope and facility spectrograph in its echelle mode (McCarthy 1988). A 1'43 \times 7'36 slit was used in combination with a (2-pixel) resolving power of $\sim 19,000$. Details on the observational strategy and data reduction are provided in Sects. 2 and 3 of White et al. (2006). White et al. (2006) also derive several stellar properties from the Palomar 60-inch spectra for these and other FEPS sources, including radial and rotational velocities, Li I λ 6708 and H α equivalent widths, chromospheric activity index R'_{HK} , and temperature- and gravity-sensitive line ratios.

The spectrum of [PZ99] J161411.0-230536 was acquired during commissioning of the East Arm Echelle spectrograph on the Hale 200-inch telescope at Palomar. The on-source exposure time was 2,000 seconds. The spectrum covers most of the 4000–9350 \AA region with a resolution that varies from 16,000 to 27,000 within each order. We extracted the spectrum and corrected for scattered

²<http://ssc.spitzer.caltech.edu/irs/calib/templ/>

³<http://ssc.spitzer.caltech.edu/legacy/fepshistory.html>

TABLE 2
LOG OF THE IRS SHORT-WAVELENGTH HIGH-RESOLUTION OBSERVATIONS.

Source	AOR Key	SH time \times ncycles	Peak-up mode
RX J1111.7-7620	5451776	31.5 \times 12	PCRS
PDS 66	5451264	6.3 \times 4	PCRS
HD 143006	9777152	6.3 \times 18	PCRS
[PZ99] J161411.0-230536	5453824	31.5 \times 4	PCRS
RX J1842.9-3532	5451521	31.5 \times 10	IRS-red
RX J1852.3-3700	5452033	121.9 \times 4	PCRS

light using custom routines in IDL, following the main steps described in White et al. (2006).

The spectrum of RX J1111.7-7620 was acquired in March 2003 with the MIKE echelle spectrograph on the Magellan Clay 6.5-m telescope (Bernstein et al. 2002). The star was observed in a 360-second exposure with the MIKE Red CCD in the standard setup with the 0.35" slit, and 2-pixel resolution of $R \simeq 36,000$ covering the wavelength range 4800–8940 Å. The data were reduced using the MIKE Redux IDL package⁴.

Finally, the spectrum of PDS 66 was acquired in April 2002 with the echelle spectrograph on the CTIO 4 meter Blanco telescope. We used the 31.6 red long echelle grating covering the wavelength range between 3,000–10,000 Å and a 0".8 \times 3".3 slit with a 2-pixel resolution of $R \simeq 45,000$. The exposure time on-source was 120 seconds. For the data reduction we used the IRAF packages *quadred/echelle* that can treat multi-amplifier echelle data.

3. Results

In Sect. 3.1 we present the gas line detections from the *Spitzer* spectra of the six FEPS optically thick dust disks. We also compute mass accretion rates from the Balmer emission profiles (Sect. 3.2) and use them in Sect. 4 to search for correlations with the flux of the detected infrared lines.

3.1. Fluxes of Infrared Gas Lines

We report the detection of [Ne II] emission at 12.81 μm in four out of the six targets and the additional detection of H I(7–6) at 12.37 μm in RX J1852.3-3700 (see Fig. 1). For these detec-

tions, we verified that the emission is centered at the expected rest wavelength, is spectrally unresolved⁵, is present in both nod1 and nod2 positions, and is absent in the sky positions. These checks guarantee that the emission originates at the source location or in its proximity, within 2".3/pixel or ~ 320 AU at a distance of 140 pc.

To estimate the fluxes of the detected lines, we fit the spectrum within $\pm 0.25 \mu\text{m}$ of each line using a Levenberg–Marquardt algorithm and assuming a Gaussian for the line profile and a first-order polynomial for the continuum. The 1σ errors on the line fluxes are evaluated from the RMS dispersion of the pixels in the spectrum minus the best fit model (see Table 3). In the case of non-detections, we fit the same spectral range with a first-order polynomial and we provide in Table 3 the 3σ upper limits to the flux from the RMS in the baseline subtracted spectrum. Figs. 1 and 2 illustrate our best fits to the detected lines (red dashed lines) and the hypothetical 3σ upper limits (light blue dot-dashed lines). In addition to the H I and the [Ne II] transitions, we provide upper limits for the [Ne III] line at 15.55 μm for which we have predicted line emissions from the X-ray and EUV models.

3.2. Mass Accretion Rates

Observational evidence for magnetospheric accretion in classical T Tauri stars (TTs) is robust (e.g. Bouvier et al. 2007). Evidence of this process are the UV/optical continuum excess, emitted by the accretion shock on the stellar surface, and permitted emission lines originating in the infalling magnetospheric gas (e.g. Muzerolle et al.

⁴<http://web.mit.edu/burles/www/MIKE>

⁵The resolving power of the SH module is $R \sim 650$ corresponding to ~ 460 km/s.

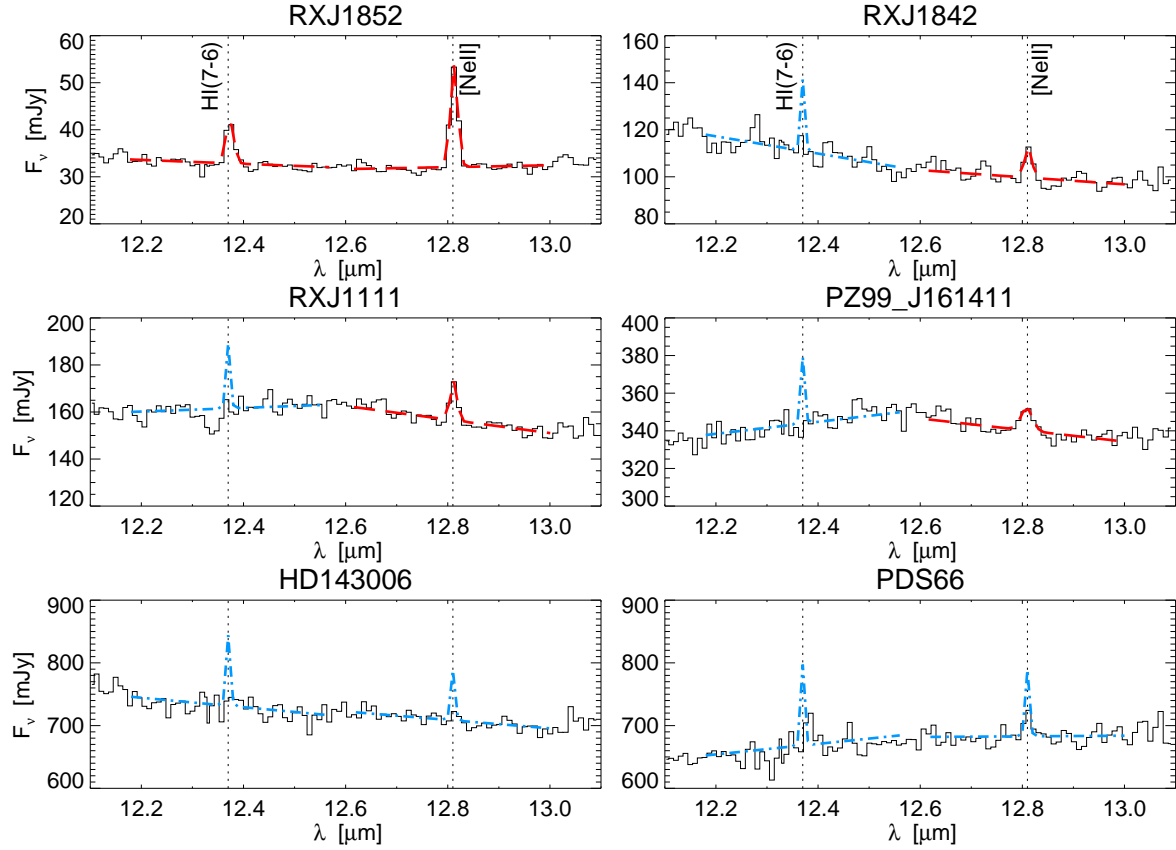


Fig. 1.— Expanded view of the wavelength regions around the H I(7–6) and [Ne II] emission lines. On top of the stellar and dust continuum we overplot the best Gaussian fits to the data (red dashed–lines) and the hypothetical 3σ upper limits (light blue dot–dashed lines) reported in Table 3. In the case of PDS 66, we might have detected [Ne II] emission at a level of $\sim 2\sigma$ (Flux $\sim 1.4 \times 10^{-14} \text{erg s}^{-1} \text{cm}^{-2}$). However, due to the faintness of the emission we cannot confirm its presence in both nod positions and therefore prefer to report a 3σ upper limit in Table 3.

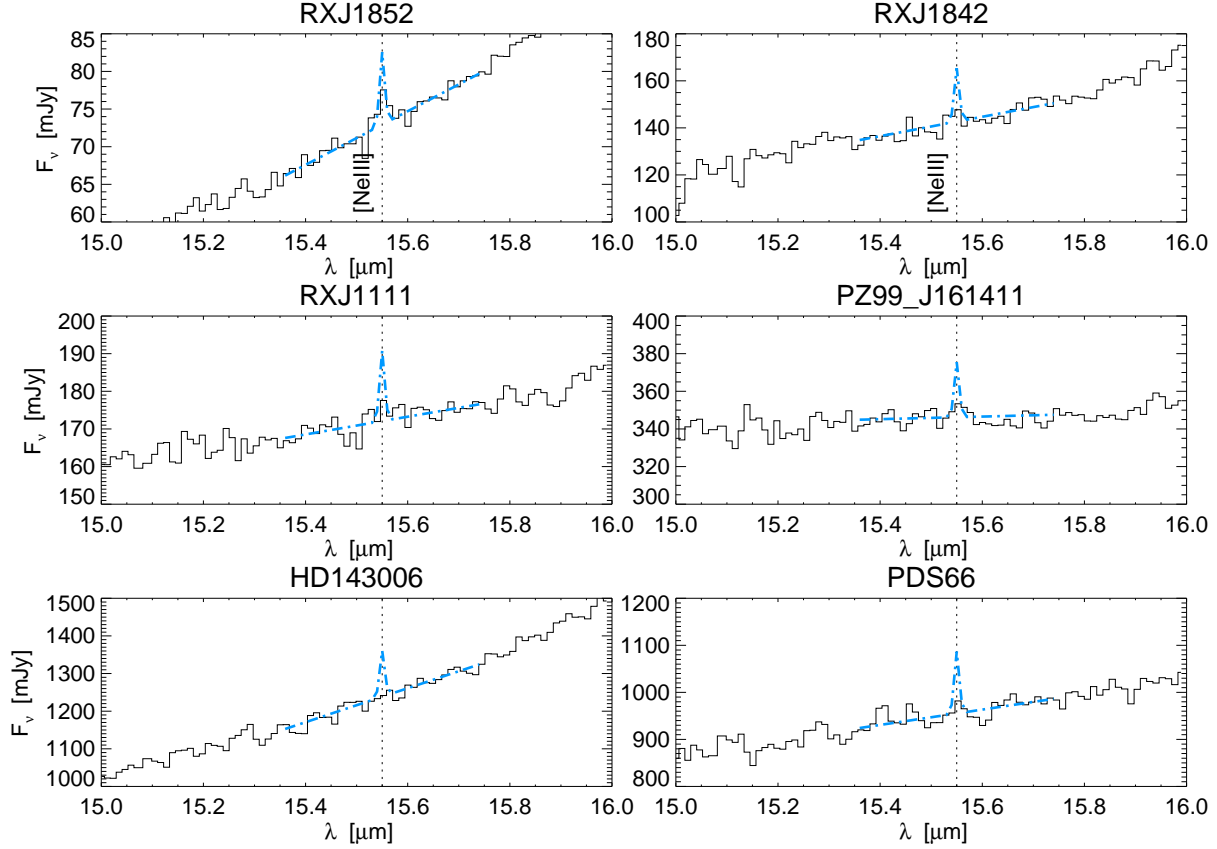


Fig. 2.— Expanded view of the wavelength regions around the [Ne III] line at $15.55 \mu\text{m}$. On top of the stellar and dust continuum we overplot the hypothetical 3σ upper limits (light blue dot-dashed lines) reported in Table 3.

TABLE 3
LINE FLUXES AND UPPER LIMITS (3σ) FROM THE IRS/SPITZER SPECTRA.

Source	Flux(H I) [$10^{-15} \text{ erg s}^{-1} \text{ cm}^{-2}$]	Flux([Ne II]) [$10^{-15} \text{ erg s}^{-1} \text{ cm}^{-2}$]	Flux([Ne III]) [$10^{-15} \text{ erg s}^{-1} \text{ cm}^{-2}$]
RX J1111.7-7620	<5.6	5.1 ± 1.2	<3.0
PDS 66	<26.0	<20.0	<21.1
HD 143006	<22.6	<15.0	<19.7
[PZ99] J161411.0-230536	<7.2	6.2 ± 1.8	<4.7
RX J1842.9-3532	<6.1	4.3 ± 1.3	<3.6
RX J1852.3-3700	3.4 ± 0.4	7.2 ± 0.4	<1.5

NOTE.—The wavelengths for the H I(7-6), [Ne II], and [Ne III] lines are 12.37, 12.81, and $15.55 \mu\text{m}$ respectively. The 1σ errors on the detections are calculated from the RMS of the observations minus model fit.

2001; Kurosawa et al. 2006). The UV/optical continuum excess emission is the most common and direct measure of mass accretion rates (\dot{M}_*). However, in many instances, this excess is too weak to be measured, and other methods such as modeling Balmer emission profiles are necessary. This is particularly true for objects with predominately low accretion rates, such as older 5–10 Myr TTSs (e.g. Muzerolle et al. 2000; Lawson et al. 2004) in the same age range as our sample.

Many diagnostics in our spectra suggest low accretion rates in comparison to values typical of younger TTSs such as in Taurus: the lack of optical continuum veiling (continuum excess over photospheric flux < 0.1), weak or absent mass loss signatures such as [O I] $\lambda 6300 \text{ \AA}$ emission, and the lack of broad emission components in the Na D doublet and Ca II triplet lines. The H α and H β emission profiles, shown in Figures 3 and 4, are in most cases qualitatively suggestive of weak accretion. One object, RX J1842.9-3532, exhibits blueshifted absorption indicative of significant mass loss, and two objects exhibit redshifted absorption components in H α ([PZ99] J161411.0-230536 and HD 143006). Given the spectral types of these stars, the lack of optical veiling implies an upper limit of $\dot{M}_* \lesssim 10^{-8} M_\odot \text{ yr}^{-1}$ (see Calvet et al. 2004).

We followed the procedures outlined in detail in Muzerolle et al. (2001) to model the Balmer line profiles and thus estimate mass accretion rates for our targets. Although the paper by Muzerolle et al. (2001) focused on low-mass stars with late K and M spectral types, accretion diagnostics such as UV excess and Pa β (Calvet et al. 2004, Natta et al. 2006) indicate that magnetospheric model assumptions can be extended to stars with early K and G spectral types like our targets. We adopted stellar parameters based on the empirically-derived quantities in Table 1. Gas temperatures were set roughly to 10,000 K following the constraints derived in Muzerolle et al. (2001). Note that for the density regime appropriate for these particular objects, the gas is already nearly fully ionized and larger gas temperatures will not result in significantly different line emission. The magnetosphere size/width was set to a fiducial value (between 2.2–3 R_*), lacking any observable constraints. This is the largest source of uncertainty in constraining the accretion rate;

however, a plausible range of values results in no more than a factor of 3–5 range in accretion rates that can reproduce the observed line profiles. We further included rotation, using the treatment of Muzerolle et al. (2001), since rotation rates typical of our objects can have an observable effect on the line profiles near the line center. The adopted stellar equatorial velocities, based on the observed $v \sin(i)$ values, are given in Table 4. Finally, the model inclination angle and mass accretion rate are varied to reproduce the wings, width, and peak of the observed lines. The best matches are shown in Figs. 3 and 4 and the inferred inclination angles (i) and mass accretion rates (\dot{M}_*) are summarized in Table 4. Note that $\dot{M}_* \lesssim 5 \times 10^{-11} M_\odot \text{ yr}^{-1}$ produce negligible H α emission for our sources and thus represent lower limits for their accretion rates. Given the magnetospheric model parameters in Table 4, we also compute the predicted flux in the H I(7–6) transition (last column of the table).

The models reasonably account for the observed profiles, with a few exceptions. The H α emission line of RX J1852.3-3700 exhibits a narrow, symmetric core that the models cannot reproduce. It is possible that there is a chromospheric emission component superposed on top of the broader accretion component. For this to occur, a significant amount of the stellar surface must not be covered by the accretion flow (which would be consistent with the more pole-on orientation of the model). The models also cannot reproduce the blueshifted absorption components seen in both H α and H β profiles of RX J1842.9-3532. A treatment of the wind is necessary to account for such features, which is beyond the scope of this work. However, we note that the models still account for the overall emission profile, suggesting that the wind produces negligible emission.

The derived mass accretion rates are all lower than the average value for 1 Myr-old T Tauri stars (Gullbring et al. 1998; Calvet et al. 2004) by factors larger than 10. Given the older ages of the stars in our sample, this may be consistent with a general decline in accretion rate with time as predicted by models of viscous disk evolution (e.g. Hartmann et al. 1998; Muzerolle et al. 2000). The predicted H I(7–6) emission for RX J1852.3-3700 contributes to at most $\sim 30\%$ of the observed

value⁶, while predicted fluxes from the other sources are negligible or fall well below the 3σ upper limits we report in Table 3. Thus, magnetospheric accretion models argue against the H I(7–6) transition originating in accretion flows. Accretion shock regions, the stellar chromosphere, and the hot disk surface are other possible sources of emission. We discuss the contribution from the disk in the next Section and note that the possible chromospheric emission component in the H α profile of RX J1852.3-3700 could also contribute to the H I(7–6) line.

4. Disk Atmosphere and [Ne II] Emission

Two-thirds of our optically thick dust disks present a [Ne II] emission line at $12.81\ \mu\text{m}$. Where does the [Ne II] emission originate? Recently Glassgold, Najita & Igea (2007) showed that stellar X-rays can partially ionize the gas in the disk atmosphere and produce detectable [Ne II] lines. Alternatively, Hollenbach & Gorti in prep. suggest that extreme ultraviolet (EUV, $h\nu > 13.6\ \text{eV}$) photons from the central star ionize the upper layer of circumstellar disks and create a kind of coronal H II region producing detectable [Ne II] emission. Although the two models rely on different ionization mechanisms, they both predict that [Ne II] emission originates from gas in a hot surface layer of circumstellar disks⁷. We can thus expect to find some correlations between the observed [Ne II] fluxes and the star/disk properties such as infrared excess emission, stellar UV or X-ray flux, and mass accretion rates.

First we explore any correlation between the continuum emission in the vicinity of the [Ne II] line and the [Ne II] line luminosities (see Fig. 5). Although there is no obvious trend between the plotted quantities, it is interesting that the four detections cluster in a narrow range of [Ne II] line luminosities (differences less than a factor of 2) and below 400 mJy of excess emission at $13\ \mu\text{m}$. The weaker mid-infrared continuum level (caused by an inner hole and/or grain growth) improves the line to continuum ratio in these relatively low

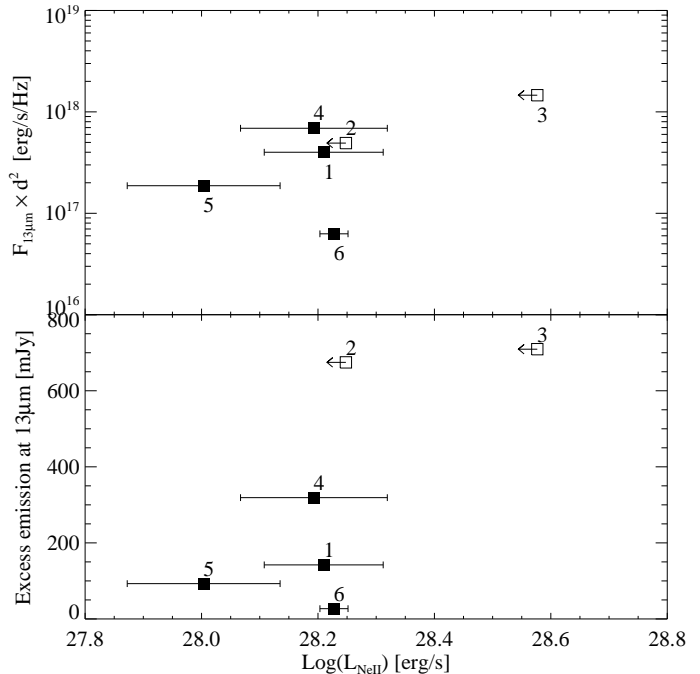


Fig. 5.— Possible correlations of [Ne II] line luminosities with disk properties. [Ne II] detections are filled squares and right-most [Ne II] limits are open squares with left pointing arrows. The numbers correspond to the ID numbers of our targets as given in Table 1. Upper panel: Dereddened flux between 12.85 and $13.15\ \mu\text{m}$ (as estimated from the low-resolution spectra, Bouwman et al. 2007) times distance squared versus the [Ne II] line luminosity. To deredden the fluxes we used the visual extinctions in Table 1 and the mean extinction law from Mathis (1990). Lower panel: Excess emission at $13\ \mu\text{m}$ versus the [Ne II] line luminosity. The excess emission is computed from the difference between the observed IRS low-resolution flux between 12.85 and $13.15\ \mu\text{m}$ and the best fit Kurucz model atmospheres (see Meyer et al. 2006 for details on the procedure) in the same wavelength range. Excess emission has been dereddened as explained above. In both plots the errorbars in the y-axis are few percent of the plotted values and thus smaller than the used symbols. Low infrared excess emission makes it more favorable to detect [Ne II] emission lines.

⁶This estimate includes a factor of 2 uncertainty in the predicted H I flux, see Note to Table 4

⁷The coronal H II region lies on top of the slightly lower X-ray heated region, which is only partially ionized (~ 0.1 to 1%).

TABLE 4

MAGNETOSPHERIC ACCRETION MODEL PARAMETERS AND RESULTING MASS ACCRETION RATES (\dot{M}_*).

Source	R_* [R_\odot]	V_{eq} [km s^{-1}]	T_{max} [K]	i [$^\circ$]	$\log(\dot{M}_*)$ [$M_\odot \text{ yr}^{-1}$]	Predicted Flux(H I) [$10^{-15} \text{ erg s}^{-1} \text{ cm}^{-2}$]
RX J1111.7-7620	2.0	25	12000	75	-9.3	0
PDS 66	1.0	0	9000	45	-8.3	2.4
HD 143006	1.5	10	12000	10	-9.3	1.3
[PZ99] J161411.0-230536	2.5	45	12000	65	-9.5	0
RX J1842.9-3532	1.0	25	10000	45	-9.0	0.48
RX J1852.3-3700	1.0	25	12000	35	-9.3	0.56

NOTE.— T_{max} is the maximum value of the adopted temperature distribution of the accretion column. All models are calculated for a solar mass star and for outer magnetospheric radii between 2.2 and $3 R_*$. The last column gives the predicted flux in the H I(7–6) transition at $12.37 \mu\text{m}$. Uncertainties in the mass accretion rates are no more than a factor of 3–5. By varying \dot{M}_* by a factor of 5 the models give a range of H I fluxes within a factor of ~ 2 .

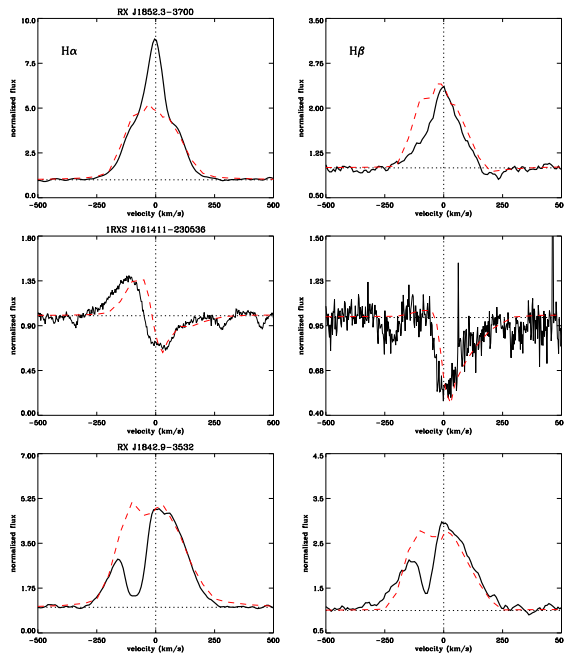


Fig. 3.— Observed and model Balmer line profiles (solid and dashed lines, respectively) for the sources RX J1852.3-3700, [PZ99] J161411.0-230536, and RX J1842.9-3532. Model parameters are listed in Table 4.

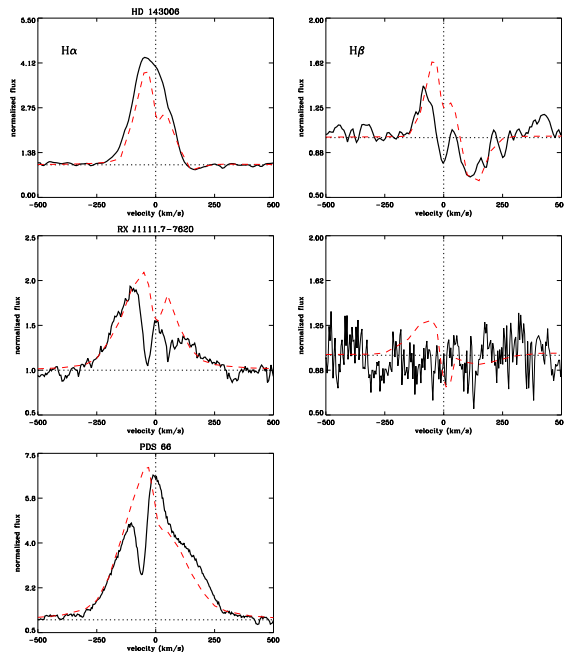


Fig. 4.— Observed and model Balmer line profiles (solid and dashed lines, respectively) for the sources HD 143006, RX J1111.7-7620, and PDS 66. Model parameters are listed in Table 4.

spectral resolution *Spitzer* observations and thus makes it more favorable to detect [Ne II] emission lines.

We also search for correlations with the disk structure, in particular with the disk flaring. The continuum flux emitted from the surface layer of the disk is proportional to the angle at which stellar radiation impinges onto the disk. This so-called grazing angle becomes proportional to the disk flaring at radial distances from solar-type stars $\gtrsim 0.4$ AU (Chiang & Goldreich 1997). Such distances are probed by dust emission at mid-infrared wavelengths. Thus, we can use the ratio of fluxes at two different mid-infrared wavelengths to trace changes in the disk flaring. We chose as reference flux that at $5.5 \mu\text{m}$, which is the shortest wavelength covered by the IRS low-resolution modules, and computed the flux ratios at 13, 24 and $33 \mu\text{m}$ (see Fig. 6). Larger flaring is indicated by higher ratios of long wavelength continuum to short wavelength continuum flux from the dust disk. Source RX J1852.3-3700 is peculiar in having small excess at $13 \mu\text{m}$ and large excesses at 24 and $33 \mu\text{m}$. The SED of this object (Silverstone et al. 2006) is reminiscent of transition systems such

GM Aur and DM Tau (Calvet et al. 2005). We do not see any obvious correlation between disk flaring and [Ne II] line luminosities.

Interestingly, we find trends with the stellar X-ray luminosities (Fig. 7) and with the mass accretion rates from the Balmer profiles (Fig. 8). Stellar X-ray luminosities are computed from the ROSAT All-Sky Survey count rates and hardness ratios (see Table 1). We did not attempt to correct for the interstellar extinction because the X-ray spectrum of our targets is not well-known from the ROSAT observations alone. Nevertheless, the largest difference in visual extinction (0.7 mag between HD 143006 and RX J1852.3-3700) translates into less than 0.1 dex difference in $\log(L_X)$, well within the estimated errors and variations due to stellar activity. This indicates that any observed trend in our sample can be only marginally influenced by the correction in interstellar extinction. The best (minimum chi-square) fit to the [Ne II] detections in Fig. 7 gives the following correlation between the [Ne II] and the X-ray luminosity:

$$L_{[\text{Ne II}]} \propto L_X^{+1.2(\pm 0.7)}$$

The slope of the relation is not constrained but

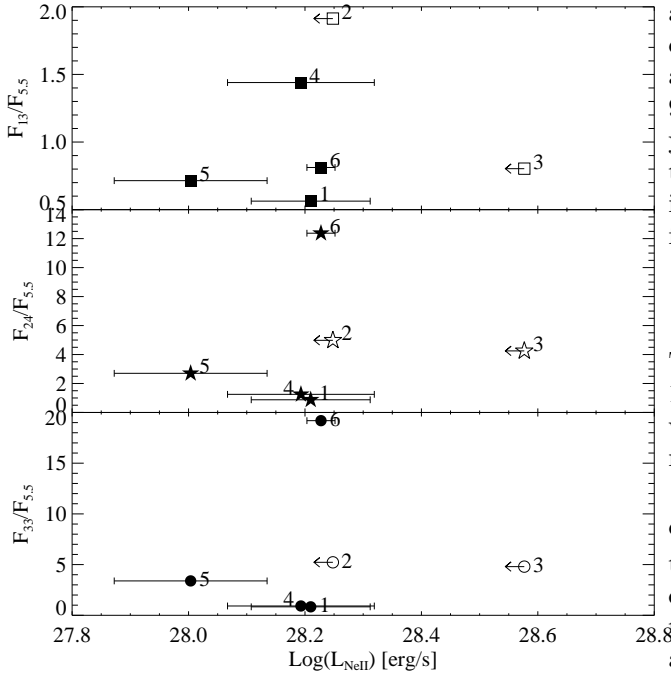


Fig. 6.— Possible correlations of [Ne II] line luminosities with the disk flaring. [Ne II] detections are filled symbols and right-most [Ne II] limits are open symbols with left pointing arrows. The disk flaring is represented by the flux ratio at 13 (upper panel), 24 (middle panel), and 33 μm (lower panel) over the reference flux at 5.5 μm , that is the shortest wavelength covered by the IRS low-resolution spectra. More flaring is indicated by higher ratios in the figure. There is no obvious correlation between disk flaring and [Ne II] emission.

it is positive within 1.5σ . To further evaluate the likelihood of a positive correlation, we generate 100 normally-distributed points around the four [Ne II] detections and fit the data using six different linear regression methods described in Isobe et al. (1990). The analytical slopes as well the average slopes of 100 random resampling of the data using bootstrap and jackknife techniques (Babu & Feigelson 1992; Feigelson & Babu 1992) are all positive. The Pearson correlation coefficient is 0.24 meaning that we can be confident of a positive correlation between $L_{[\text{Ne II}]}$ and L_X at a 95% confidence level. We perform a similar analysis to test the apparent anti-correlation between the [Ne II] luminosity and the mass accretion rate in Fig. 8. The ordinary least-squares fit to the four [Ne II] detections results in:

$$L_{[\text{Ne II}]} \propto \dot{M}_*^{-0.45(\pm 0.36)}$$

The slope of the relation is negative only within 1σ . The Monte Carlo approach in combination with the six regression methods also indicates a negative correlation at a 95% confidence level.

In summary, we have evidence for a positive correlation between $L_{[\text{Ne II}]}$ and L_X and a negative correlation between $L_{[\text{Ne II}]}$ and \dot{M}_* . However we cannot quantify the slopes of these relations because of the small number of detections and of the large errorbars in the measured and estimated quantities. It is also important to point out that source 5 (RX J1842.9-3532) has a large weight in determining these trends being the target with the most different X-ray luminosity and mass accretion rate. Note that if the 2σ detection from PDS 66 is real it would confirm the positive trend between [Ne II] luminosity and X-ray luminosity. A larger sample of sources spanning a wider range in X-ray luminosities and mass accretion rates is necessary to constrain the slopes of the $L_{[\text{Ne II}]}-L_X$ and $L_{[\text{Ne II}]}-\dot{M}_*$ relations. In the subsections below we discuss predictions from the X-ray and EUV models and compare them to the measured [Ne II] fluxes and to the correlations presented in this Section.

4.1. Plausible Disk Origin for the Ne^+ emission

According to the model proposed by Glassgold, Najita & Igea (2007), detectable [Ne II] emission can be pro-

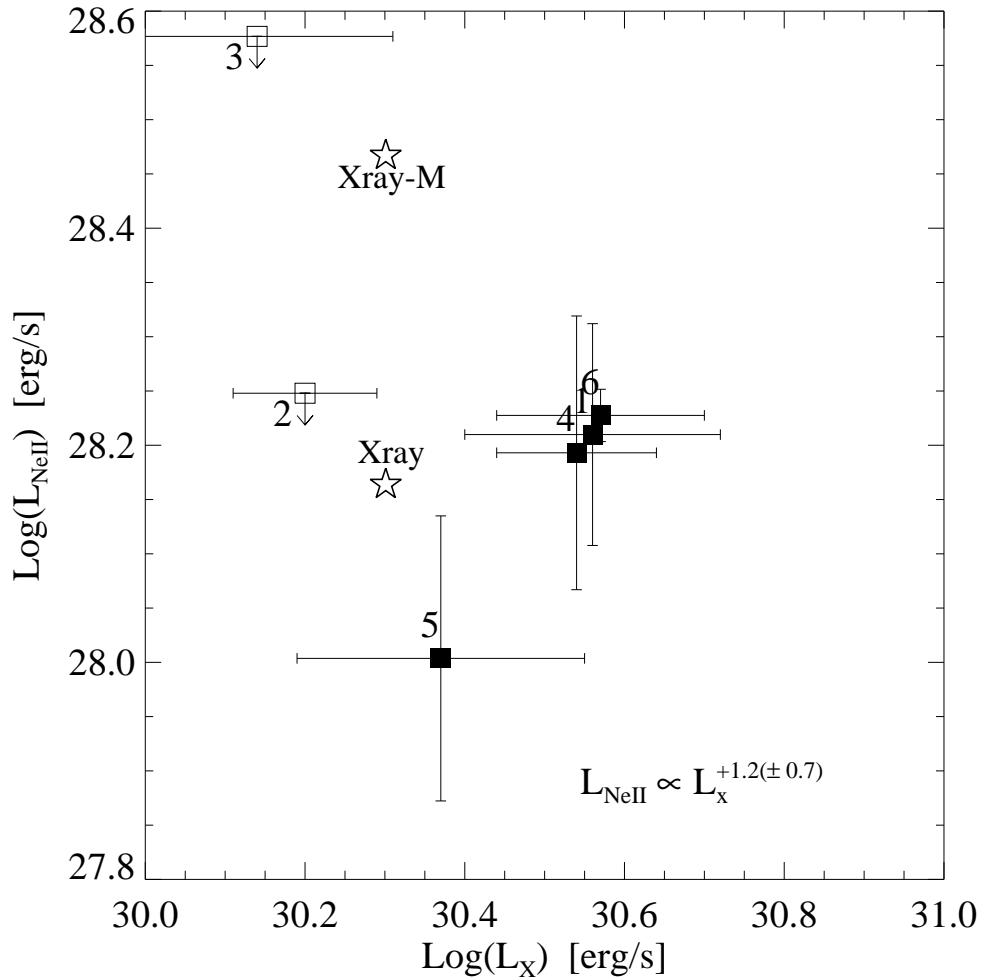


Fig. 7.— Line luminosities (filled symbols) and upper limits (open symbols with downward arrows) for the [Ne II] transition versus the star X-ray luminosity as given in Table 1. The two open stars represent the two extreme thermal models from Glassgold, Najita & Igea (2007): the upper model is when mechanical heating (accretion) dominates (Xray-M), the lower model is when X-ray heating dominates (Xray). The ordinary least-squares fit to the four detections suggests a positive correlation between $L_{[\text{Ne II}]}$ and L_X .

duced by the atmosphere of a disk both ionized and heated by stellar X-rays (Glassgold, Najita & Igea 2004). Ne ions, primarily Ne^+ and Ne^{2+} , are generated through X-ray ionization and destroyed by charge exchange with atomic hydrogen and radiative recombination. Because the X-rays emitted by young stars have a characteristic energy similar to the K-edges of Ne and Ne^+ at $\sim 0.9\text{keV}$, they are efficient in producing Ne ions. The warm disk surface region ($T \sim 4000\text{K}$) generated by X-ray irradiation extends out to large radii ($\sim 20\text{AU}$). As a result, fine structure transitions of Ne^+ and Ne^{2+} , which have excitation temperatures of $\sim 1000\text{K}$, can be produced over a vertical column of warm gas of $10^{19} - 10^{20}\text{cm}^{-2}$ and over a large range of disk radii. These circumstances lead to a significant flux of [Ne II] at $12.81\mu\text{m}$ and [Ne III] at $15.55\mu\text{m}$.

For a typical T Tauri disk (D’Alessio et al. 1999) located at 140 pc, Glassgold, Najita & Igea (2007) predict that a stellar X-ray luminosity of $\log(L_X) = 30.30\text{ergs}^{-1}$ generates a [Ne II] flux of $6.22 \times 10^{-15}\text{ergs}^{-1}\text{cm}^{-2}$ when accretion related processes are unimportant in heating the disk surface. The [Ne III] flux is estimated to be approximately 10 times lower. The X-ray luminosity assumed in the Glassgold et al. model is close to that of RX J1842.9-3532 (see Table 1 and Fig. 7) and the predicted [Ne II] flux is similar (within a factor of 1.5) to the value we report in Table 3. Unfortunately, the upper limits on the [Ne III] lines (see Table 3) are not stringent enough to test the model predictions.

In the model proposed by Hollenbach & Gorti (2007, in preparation), EUV photons from the stellar chromosphere (Alexander et al. 2005) and/or from accretion (Matsuyama et al. 2003; Herczeg et al. 2007) create an H II-region like ionized layer on the surface of young circumstellar disks. The EUV photons incident on the disk are mostly absorbed near the so-called ”gravitational radius” ($\sim 10\text{AU}$ for a 1M_\odot star) where the local thermal speed of the 10^4K ionized hydrogen nuclei is equal to the escape speed from the gravitational potential (e.g. Hollenbach et al. 1994). The numerical model for the EUV-heated disk surfaces includes a calculation of the diffuse field due to hydrogen and helium recombinations, and ionized gas chemistry comprising photoionizations, recombinations, and charge exchange reactions (Hollenbach & Gorti

2007, in prep.). In the case of a soft EUV spectrum (e.g. a blackbody at $4 \times 10^4\text{K}$), photon luminosities of $\sim 10^{41}\text{ergs}^{-1}$ produce a [Ne II] line luminosity of $\sim 10^{-6}L_\odot$, which corresponds to a flux of $2 \times 10^{-15}\text{ergs}^{-1}\text{cm}^{-2}$ from a source at 140 pc. Harder EUV spectra can produce more doubly ionized Ne in the disk atmosphere which may result in stronger [Ne III] lines in comparison to the case of soft EUV spectra (Hollenbach & Gorti 2007, in prep.).

With the assumption that Ne atoms are ionized only by stellar EUV photons and that the sources have a soft EUV spectrum, one can use [Ne II] lines as an indirect tool to estimate EUV fluxes⁸, which are unconstrained for the majority of the stars. The [Ne II] fluxes we report in Table 3 convert to EUV fluxes between 2.6×10^{41} (for RX J1842.9-3532) and 4.4×10^{41} (for RX J1852.3-3700) photons s^{-1} . Such ionizing rates seem plausible for $\sim 5\text{Myr}$ old TTSs like our targets. For comparison Herczeg et al. (2007) calculate $\sim 10^{41}$ ionizing photons s^{-1} for the $\sim 10\text{Myr}$ old TW Hya system while Alexander et al. (2005) estimate a wide range of ionizing fluxes $\sim 10^{41} - 10^{44}$ photon s^{-1} for a sample of five classical T Tauri stars. The estimates from Alexander et al. (2005) are based on modeling UV emission lines such as C IV and have only an order of magnitude accuracy due to model uncertainties and more significantly to uncertainties in the reddening. Nevertheless, if X-rays contribute to ionize Ne atoms, as proposed by Glassgold, Najita & Igea (2007), our EUV estimates from [Ne II] lines can be only taken as upper limits.

In summary, both the X-ray and the EUV models can reproduce the observed [Ne II] line luminosities with star/disk properties that are plausible for our targets. Can the same models explain the H I(7-6) flux from RX J1852.3-3700? Hollenbach & Gorti estimate that $L_{\text{H I}} \sim 10^{-3}L_{[\text{Ne II}]}$ if all the H I(7-6) emission originates from the ionized disk surface. They show that if X-rays dominate the [Ne II] emission, then the H I luminosity should be even lower because the gas is mostly neutral. This demonstrates that neither the EUV nor the X-ray models can account for the observed

⁸In the EUV model the [Ne II] luminosity is directly proportional to the EUV luminosity of sources with soft EUV spectra

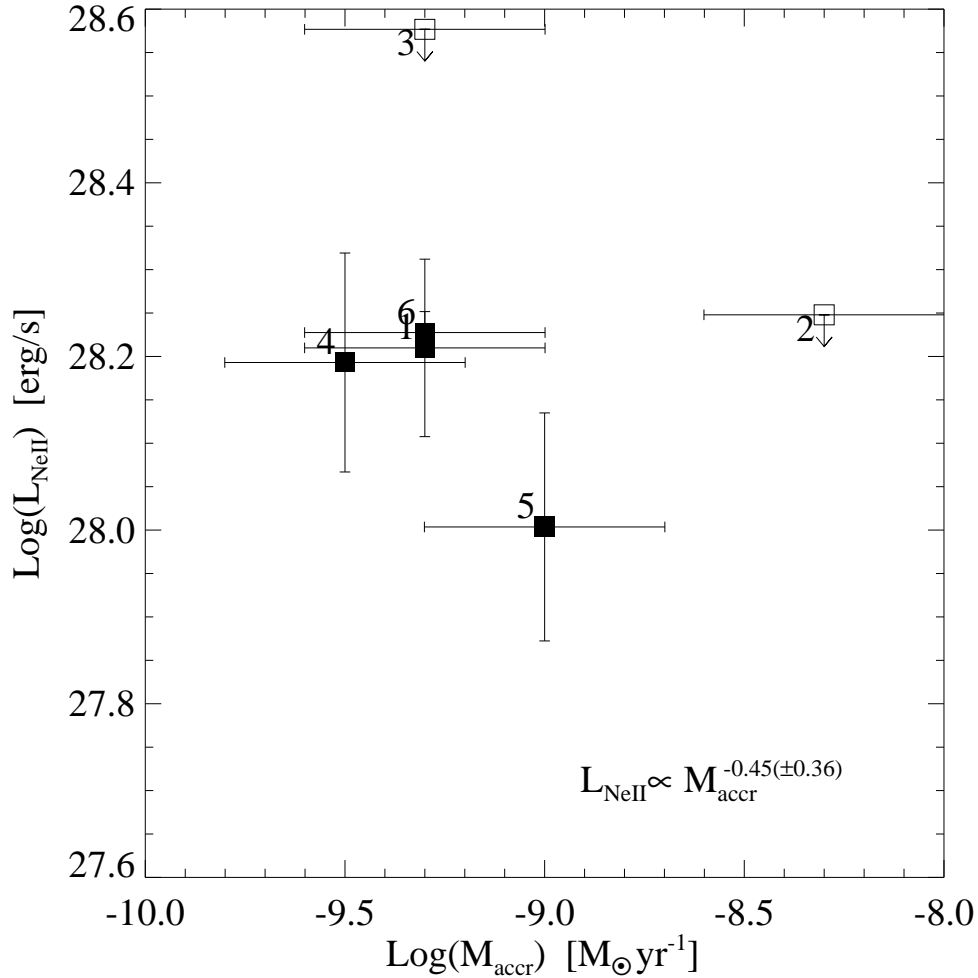


Fig. 8.— Line luminosities (filled symbols) and upper limits (open symbols with downward arrows) for the [Ne II] transition versus the stellar accretion rates given in Table 4. We overplot a factor of 4 uncertainty in the mass accretion rates, representative of the uncertainties we estimate from the models (see Sect. 3.2). The ordinary least-squares fit to the four detections suggests an anti-correlation between $L_{[\text{Ne II}]}$ and \dot{M}_{\star} .

H I flux, which is only a factor of ~ 2 lower than the [Ne II] flux. We conclude that the H I(7–6) transition is not associated with either the X–ray excited gas or the EUV excited gas in the disk. Because magnetospheric accretion flows can account for at most $\sim 30\%$ of the observed H I(7–6) flux (Sect. 3.2), accretion shocks and/or the stellar chromosphere are left as possible major sources of emission.

4.2. Predicted Correlations and Observed Trends

In this subsection we discuss whether the trends identified in Sect. 4 are consistent with predictions from the X–ray and EUV models.

First we consider the correlation between the [Ne II] luminosity and the X–ray luminosity. The X–ray model predicts that the ionization fraction of Ne atoms is proportional to the square root of the stellar X–ray luminosity: $x(\text{Ne}^+)/x(\text{Ne}) \propto L_X^{1/2}$ (eqs. 2.9 and 2.10 from Glassgold, Najita & Igea 2007). The integrated flux of the [Ne II] line further depends on the excitation of the line, which is a function of the disk temperature and electron density. Further modeling by Meijerink, Glassgold & Najita in prep. indicate that there is a close to linear relation between $L_{[\text{Ne II}]}$ and L_X , which is consistent with the positive correlation suggested by our data. This trend could be also consistent with the EUV model. In the case of a soft EUV spectrum, most of the Ne in the disk surface is Ne^+ and the [Ne II] luminosity is predicted to be directly proportional to L_{EUV} (Hollenbach & Gorti 2007 in prep.). What is the relation between L_{EUV} and L_X ? Emission lines such as C IV and O VI tracing the EUV emission are found to scale with the X–ray flux with power law indices close to 0.5 in $\sim \text{Gyr}$ old sun–like stars (Ayres 1997; Guinan et al. 2003). If these relations hold for younger sun–like stars then the EUV model would also predict a positive correlation between $L_{[\text{Ne II}]}$ and L_X .

Glassgold, Najita & Igea (2007) also explored the effect of accretion heating on the [Ne II] flux. Accretion at a level of $10^{-8} M_\odot \text{yr}^{-1}$, which is typical for a classical TTS, results in a factor of 2 higher [Ne II] flux than that produced by a non-accreting TTS surrounded by the same circumstellar disk (see also Fig. 7). This suggests a mild pos-

itive correlation between $L_{[\text{Ne II}]}$ and \dot{M}_* , which is different from the one we see in our data (Sect. 4 and Fig. 8). However a detailed comparison with the models needs to take into account other factors in addition to stellar accretion such as disk flaring and inclination. In the case of the EUV model, stellar winds greater than $\sim 10^{-10} M_\odot \text{yr}^{-1}$ could drastically reduce the EUV photons reaching the disk (Hollenbach & Gorti in prep.). Given that the ratio of mass outflow rate to the mass accretion rate is close to ~ 0.1 for most classical TTSs with a large uncertainty (Shu et al. 2000; White & Hillenbrand 2004), these wind rates correspond to $\dot{M}_* \gtrsim 10^{-9} M_\odot \text{yr}^{-1}$. Thus, the EUV model predicts significantly lower [Ne II] luminosities for classical TTSs simply due to their higher accretion (and thus wind) rates.

Finally, disk flaring is also expected to play a major role in the X–ray model in that more flaring facilitates the penetration of stellar X–ray in the disk atmosphere (Glassgold, Najita & Igea 2007). On the contrary, the [Ne II] emission produced by EUV photons is expected to be independent of the disk flaring (Hollenbach & Gorti in prep.). Quantitative predictions from both models are necessary before attempting any comparison with the empirically derived signature of disk flaring presented in Fig. 6.

5. Discussion

We have shown in the previous Sections that both the X–ray and EUV models can account for the observed [Ne II] fluxes suggesting that the emission originates in the hot disk atmosphere. Other sources of [Ne II] emission that we have not discussed so far might be a jet or an outflow. In this case, the jet/outflow needs to provide enough energy to ionize Ne atoms, i.e. about twice the energy to ionize atoms like S and N whose forbidden lines are sometimes detected in classical TTSs (Hartigan et al. 1995). Our sources however have very weak or absent mass loss signatures and accretion rates at least a factor of 10 lower than those of typical TTSs (see Sect. 3.2). Thus, we regard the possibility of a jet/outflow dominating the [Ne II] emission as very unlikely for our targets.

It is possible to confirm that [Ne II] emission originates from the disk atmosphere by spectrally resolving the detected lines. High–resolution spec-

troscopy could also enable the detection of the weaker [Ne III] line that can be used to further test the model predictions. Emission arising from disk radii out to ~ 10 AU around a solar mass star would produce a line with ~ 10 km/s width, about 40 times smaller than the spectral resolution of the *Spitzer* IRS. Current ground-based spectrographs with spectral resolutions $R \gtrsim 30,000$ at $12\ \mu\text{m}$ such as VISIR/VLT and TEXES/Gemini should be able to resolve such emission lines. In addition similar observations of the H I(7-6) line at $12.37\ \mu\text{m}$ could confirm that the H I line originates in a different region from the [Ne II] line.

However high-resolution spectroscopy alone is not sufficient to identify whether X-rays or EUV photons dominate the ionization of Ne atoms. In fact both the X-ray and EUV model predict a similar extension of the [Ne II] emitting region. Constraints for the EUV model can come from independent estimates of the stellar EUV flux. Because EUV emission is produced by gas at temperatures between $10^5 - 10^6$ K, an estimate of the emitting plasma can be achieved by using gas lines such as the O VI tracing gas at intermediate temperatures. An important parameter in the X-ray model is the input X-ray luminosity and spectral temperature which Glassgold, Najita & Igea (2007) take from solar-like young stellar objects in Orion (Wolk et al. 2005). It will be important to explore the effect of different X-ray luminosities and spectra to better compare model predictions with observations. The anti-correlation between [Ne II] luminosity and mass accretion rate (if confirmed by a larger sample of sources) could be used to identify the dominant ionization mechanism for Ne atoms. Detections of [Ne II] emission lines from classical TTSs, older TTSs, and young brown dwarfs will help sample the trend to mass accretion rates ranging from $\sim 10^{-8}$ down to $\sim 10^{-10} M_{\odot} \text{ yr}^{-1}$.

None of the optically thin systems we published in Pascucci et al. (2006) exhibits [Ne II] emission at $12.81\ \mu\text{m}$. The majority of these sources have 3σ line flux upper limits in the H₂S(2) line (that are representative for the [Ne II] lines) about an order of magnitude lower than the [Ne II] fluxes we detect in the four optically thick disks (see Table 4 in Pascucci et al. 2006). In addition, these optically thin systems span a wide range in X-ray luminosities that covers the X-ray luminosities

of the sources with detected [Ne II] emission. This indicates that the optically thin sample in Pascucci et al. (2006) lack enough hot gas to emit detectable [Ne II] emission. The EUV and X-ray models of optically thick dust disks as presented above can reproduce the observed [Ne II] emission lines from only $\sim 6 \times 10^{-7} M_J$ of gas within 10 AU or $\sim 3 \times 10^{-5} M_J$ of gas within 20 AU, respectively. Thus, [Ne II] non-detections in optically thin systems might be used to set even more stringent gas mass upper limits than those we reported in Hollenbach et al. (2005) and Pascucci et al. (2006) using other mid-infrared gas transitions. However, a correct determination of the gas mass upper limits requires detailed modeling of the star/disk properties. We plan to explore this issue in a separate contribution.

6. Summary

To summarize, the main conclusions of this paper are as follows:

1. We detect [Ne II] emission lines at $12.81\ \mu\text{m}$ in four out of six optically thick dust disks observed as part of the FEPS *Spitzer* Legacy program. The systems with [Ne II] emission are characterized by weaker mid-infrared continuum (possibly the result of an inner hole and/or grain growth) compared to those systems where we do not detect [Ne II] lines.
2. We also detect a H I(7-6) emission line from RX J1852.3-3700. Magnetospheric accretion flows can account for at most $\sim 30\%$ of the observed flux. This line is not associated with the gas emitting the [Ne II] lines. Accretion shocks and/or the stellar corona could contribute to most of the observed H I(7-6) emission.
3. The [Ne II] line luminosity correlates with the stellar X-ray luminosity. We find an anti-correlation between the [Ne II] luminosity and the mass accretion rate. The slopes of these trends are not constrained by the current data.
4. Emission from Ne⁺ is very likely arising from the hot surface of the disk. Both stellar X-rays and EUV photons can sufficiently ionize

the disk surface to reproduce the observed line fluxes.

It is a pleasure to thank all members of the FEPS team for their contributions to the project and to this study. IP wishes to thank D. Watson for suggestions in the data reduction of the IRS high-resolution spectra and A. E. Glassgold for helpful discussions on the X-ray model predictions. We thank the referee Dmitry Semenov for a very helpful review. This work is based on observations made with the Spitzer Space Telescope, which is operated by the Jet Propulsion Laboratory, California Institute of Technology under NASA contract 1407. FEPS is pleased to acknowledge support through NASA contracts 1224768, 1224634, and 1224566 administered through JPL.

Facilities: Spitzer Space Telescope

REFERENCES

- Alcalá, J. M., Krautter, J., Schmitt, J. H. M. M., Covino, E., Wichmann, R., Mundt, R. 1995, *A&AS*, 114, 109
- Alcalá, J. M., Krautter, J., Covino, E., Neuhaeuser, R., Schmitt, J. H. M. M., Wichmann, R. 1997, *A&A*, 319, 184
- Alexander, C. M. O'd., Boss, A. P., Keller, L. P., Nuth, J. A., Weinberger, A. 2007, 801, in *Protostars and Planets V*, ed. B. Reipurth, D. Jewitt, & K. Keil (Tucson: Univ. Arizona Press)
- Alexander, R. D., Clarke, C. J., Pringle, J. E. 2005, *MNRAS*, 358, 283
- Apai, D., Pascucci, I., Bouwman, J., Natta, A., Henning, Th., Dullemond, C. P. 2005, *Science*, 310, 834
- Ayres, T. R. 1997, *JGR*, 102, 1641
- Babu, G. J. & Feigelson, E. D. 1992, *Comm. in Statistics, Simulation & Computation*, 21, 533
- Bernstein, R., Shtetman, S., Gunnels, S., Mochnacki, S., Athey, A. 2002, *Proc SPIE* 4841
- Bouvier, J., Alencar, S. H. P., Harries, T. J., Johns-Krull, C. M., & Romanova, M. M. 2007, 479, in *Protostars and Planets V*, ed. B. Reipurth, D. Jewitt, & K. Keil (Tucson: Univ. Arizona Press)
- Bouwman, J., Meeus, G., de Koter, A., Hony, S., Dominik, C., Waters, L. B. F. M. 2001, *A&A*, 375, 950
- Bouwman, J., Henning, Th., Hillenbrand, L. A., Meyer, M. R., Pascucci, I., Carpenter, J. M., Hines, D. C., Kim, J. S., Silverstone, M. D. 2007, *ApJ*, submitted
- Calvet, N., Muzerolle, J., Briceño, C., Hernández, J., Hartmann, L., Saucedo, J. L., & Gordon, K. D. 2004, *AJ*, 128, 1294
- Calvet, N., D'Alessio, P., Watson, D. M. et al. 2005, *ApJ*, 630L, 185
- Chiang, E. I. & Goldreich, P. 1997, *ApJ*, 490, 368
- Cutri, R. M., Skrutskie, M. F., van Dyk, S. et al. 2003, *2MASS All Sky Catalog of point sources*
- D'Alessio, P., Calvet, N., Hartmann, L., Lizano, S., Cantó, J. 1999, *ApJ*, 527, 893
- de Zeeuw, P. T., Hoogerwerf, R., de Bruijne, J. H. J., Brown, A. G. A., Blaauw, A. 1999, *AJ*, 117, 354
- Feigelson, E. D. & Babu, G. J. 1992, *ApJ*, 397, 55
- Fleming, T. A., Molendi, S., Maccacaro, T., Wolter, A. 1995, *ApJS*, 99, 701
- Glassgold, A. E., Najita, J., Igea, J. 2004, *ApJ*, 615, 972
- Glassgold, Najita & Igea 2007, *ApJ*, 656, 515
- Gorti, U. & Hollenbach, D. 2007, in prep.
- Guinan, E. F., Ribas, I., Harper, G. M. 2003, *ApJ*, 594, 561
- Gullbring, E., Hartmann, L., Briceño, C., & Calvet, N. 1998, *ApJ*, 492, 323
- Hartigan, P., Edwards, S., Ghandour, L. 1995, *ApJ*, 452, 736
- Hartmann, L., Calvet, N., Gullbring, E., & D'Alessio, P. 1998, *ApJ*, 495, 385
- Herczeg, G. J. et al. 2007, in prep.
- Hollenbach, D., Johnstone, D., Lizano, S., Shu, F. 1994, *ApJ*, 428, 654

- Hollenbach, D., Gorti, U., Meyer, M., Kim, J. S., Morris, P., Najita, J., Pascucci, I., Carpenter, J., Rodmann, J., Brooke, T., Hillenbrand, L., Mamajek, E., Padgett, D., Soderblom, D., Wolf, S., Lunine, J. 2005, *ApJ*, 631, 1180
- Houk, N. & Smith-Moore, M. 1988, *Michigan Spectral Survey*, vol. 4
- Isobe, T., Feigelson, E. D., Akritas, M. G., Babu, G. J. 1990, *ApJ*, 364, 104
- Kurosawa, R., Harries, T. J., & Symington, N. H. 2006, *MNRAS*, 370, 580
- Lawson, W. A., Lyo, A., & Muzerolle, J. 2004, *MNRAS*, 351, L39
- Luhman, K. L. 2007, "Handbook on nearby star-forming regions", Ed. B. Reipurth
- Mamajek, E. E., Meyer, M. R., Liebert, J. 2002, *AJ*, 124, 1670
- Marino, A., Micela, G., Peres, G., Sciortino, S. 2003, *A&A*, 406, 629
- Mathis, J. S. 1990, *ARA&A*, 28, 37
- Matsuyama, I., Johnstone, D., Hartmann, L. 2003, *ApJ*, 582, 893
- McCarthy, J. K. 1988, Ph.D. thesis, California Institute of Technology
- Meyer, M. R., Hillenbrand, L. A., Backman, D. et al. 2006, *PASP*, 118, 1690
- Muzerolle, J., Hillenbrand, L., Calvet, N., Hartmann, L., & Briceño, C. 2000, *ApJ*, 545, L141
- Muzerolle, J., Calvet, N., & Hartmann, L. 2001, *ApJ*, 550, 944
- Natta, A., Testi, L., Randich, S. 2006a, *A&A*, 452, 245
- Natta A., Testi, L., Calvet, N., Henning, Th., Waters, R., Wilner, D. 2007, 767, in *Protostars and Planets V*, ed. B. Reipurth, D. Jewitt, & K. Keil (Tucson: Univ. Arizona Press)
- Neuhäuser, R., Walter, F. M., Covino, E., Alcalá, J. M., Wolk, S. J., Frink, S., Guillout, P., Sterzik, M. F., Comerón, F. 2000, *A&AS*, 146, 323
- Neuhäuser, R. & Forbrich, J. 2007, "Handbook on nearby star-forming regions", Ed. B. Reipurth
- Pascucci, I., Gorti, U., Hollenbach, D., Najita, J., Meyer, M. R., Carpenter, J. M., Hillenbrand, L. A., Herczeg, G. J., Padgett, D. L., Mamajek, E. E., Silverstone, M. D., Schlingman, W. M., Kim, J. S., Stobie, E. B., Bouwman, J., Wolf, S., Rodmann, J., Hines, D. C., Lunine, J., Malhotra, R. 2006, *ApJ*, 651, 1177
- Preibisch, T., Guenther, E., Zinnecker, H., Sterzik, M., Frink, S., Roeser, S. 1998, *A&A*, 333, 619
- Preibisch, T., Brown, A. G. A., Bridges, T., Guenther, E., Zinnecker, H. 2002, *AJ*, 124, 404
- Sciortino, S., Damiani, F., Favata, F., Micela, G. 1998, *A&A*, 332, 825
- Shu, F. H., Najita, J. R., Shang, H., Li, Z.-Y. 2000, *Protostars and Planets IV*, p. 789
- Silverstone, M. D., Meyer, M. R., Mamajek, E. E., Hines, D. C., Hillenbrand, L. A., Najita, J., Pascucci, I., Bouwman, J., Kim, J. S., Carpenter, J. M., Stauffer, J. R., Backman, D. E., Moro-Martin, A., Henning, T., Wolf, S., Brooke, T. Y., Padgett, D. L. 2006, *ApJ*, 639, 1138
- Sylvester, R. J., Skinner, C. J., Barlow, M. J., Mannings, V. 1996, *MNRAS*, 279, 915
- Voges, W., Aschenbach, B., Boller, Th. et al. 1999, *A&A*, 349, 389
- Voges, W., Aschenbach, B., Boller, Th. et al. 2000, *IAUC*, 7432R, 1
- White, R. J. & Hillenbrand, L. A. 2004, *ApJ*, 616, 998
- White, R. J., Gabor, J., & Hillenbrand, L. A. 2006, *AJ*, in press
- Wolk S. J., Harnden, F. R. Jr., Flaccomio, E., Micela, G., Favata, F., Shang, H., Feigelson, E. D. 2005, *ApJS*, 160, 423
- Wooden, D., Desch, S., Harker, D., Gail, H.-P., Keller, L. 2007, 815, in *Protostars and Planets V*, ed. B. Reipurth, D. Jewitt, & K. Keil (Tucson: Univ. Arizona Press)

